Design of Electromagnetic Wave Multi-Type Focusing Based on 1-bit Metasurface

Honggang Hao, Sen Zheng*, Yihao Tang, and Xuehong Ran

Abstract—Aiming at the focusing of near-field electromagnetic (EM) energy, a design approach of multi-type focusing (MTF) based on 1-bit metasurface is proposed in this paper. The surface electric field required for multi-focus is actually obtained by the superposition of the surface electric field of each single focus. This method can flexibly design the number, position, and energy distribution ratio of the focus according to the phase arrangement of the metasurface. Dipole structure is used as "0" and "1" unit of 1-bit metasurface. The phase difference of reflection is 180°, and the reflection coefficient is over 90% in 7.4–21.9 GHz. Using this 1-bit unit, the linear focus metasurface, multi-focus metasurface, and metasurface generating two foci with different energy distribution are realized respectively. The energy distribution metasurface was manufactured and measured, and the measured results are consistent with the simulations. The design method used in this paper is simple and effective to realize multi-focus metasurface design and has potential application value in microwave imaging, radio frequency identification (RFID), and wireless power transmission.

1. INTRODUCTION

Electromagnetic (EM) wave focusing refers to the convergence of EM energy to the receiving area, which has a wide range of applications in optical imaging [1], RFID [2], biomedicine, and other fields [3, 4]. In the optical frequency band, the general method of EM focusing is to use a dielectric lens to focus plane wave or spherical wave [5]. The dielectric constant and permeability in the medium are uniform and isotropic, and the phase accumulation is achieved by the optical path of the EM wave propagating in the medium. In the microwave frequency band, if the dielectric lens is adopted as a focusing device, it will have disadvantages such as large volume, large loss, and difficult manufacture. In addition to dielectric lens, array antenna is used in achieving the effect of near-field focusing by changing the arrangement mode of array antenna and the phase-shifting network loaded at its front end [6]. The control network of array antenna in this method is complex, and it is difficult to realize the energy distribution of each focus. As a two-dimensional artificial EM structure, metasurface can manipulate the amplitude [7], frequency [8], polarization [9], and phase of EM waves [10]. It also has the advantages of low profile and ease of fabricated [11, 12]. The metasurface changes the EM propagation path by means of phase discontinuity. If the EM wave is reflected from the metasurface to a set region, the EM focusing can be achieved. Two orthogonal line-polarization phase responses are independently designed to realize dual-polarization multi-focus focusing [13, 14]. Based on the analysis of chiral metamaterials, broadband cross-polarization single focus focusing is realized [15]. In practical applications, the type of focus needs to be designed according to the requirements [16], especially the number of foci and the position of each focus. Focusing metasurface is developing towards the trend of adjustable focus quantity and distributable energy [17].

In 2014, the digital coding metasurfaces was proposed and introduced into the design of the metasurface. For the simplest 1-bit encoding, the phase difference between the units is 180° [18]. If the phase gradient is designed according to 90° and 45°, respectively, 2-bit and 3-bit coding can be realized. For 1-bit focusing metasurface, the reflection units have only two states, "0" and "1". The 1-bit encoding method is also applied in antenna design. For example, a 1-bit coding resonator plate is used to reduce the coupling of crossed dipole antennas in [19]. To manipulate the radiation characteristics of monopole antennas, 152 different groundplane configurations are created by using 1-bit encoding method in [20]. Because the number of units required by the 1-bit analysis method is only two, the complexity of the system is reduced. The above-mentioned works are all analyzed by a 1-bit configuration. A thin planar printed phase correcting surface was designed to improve aperture phase distribution and hence the directivity pattern of electromagnetic band gap resonator antennas [21]. A multifunctional coding metasurface is proposed with functionalities controlled by both incident frequency and polarization [22]. At present, the multi-focus electromagnetic focusing characteristics of metasurfaces have not been explored in detail by using 1-bit analysis methods.

In this paper, 1-bit digital coding is introduced into the design of focusing metasurface, and the design of phase distribution is transformed into the design of "0" and "1" coding sequences. The dipole structure is used as the metasurface unit, and the near-field linear focus, point focus, and multi-focus energy distribution are analyzed and studied, respectively. In order to verify the correctness of the theory and simulation, the bifocal metasurface is fabricated and measured. The measurement results are in good agreement with the design. Research shows that not only the metasurface designed by this method can realize multi-focus, but also the position and energy of each focus can be set according to the demand.

2. DESIGN METHOD

The principle of metasurface focusing can be explained by the generalized Snell's law. The incident EM wave is reflected by the metasurface. Due to the phase mutation introduced by the metasurface, the propagation direction of the EM wave will change. If the metasurface phase distribution is calculated according to the law of focusing, the reflected EM waves can be concentrated into focus.

For a single focus metasurface, the phase at the focus point is ahead of the phase at metasurface when the metasurface is taken as the reference plane. Thus the phase distribution of the single focus metasurface can be expressed as

$$\Delta\phi(x_i, y_i) = \arg\left\{ A\exp\left(-j\frac{2\pi}{\lambda}|F - r_i|\right)\right\} \tag{1}$$

where A is the amplitude of the electric field, λ the wavelength, F the focal length, and x_i and y_i are the unit coordinates. Under ideal circumstances, we can specify the focus to be the coordinates of any position on one side of the reflection plane.

For the multi-focus metasurface, the total surface electric field distribution is actually obtained by the vector superposition of the required surface electric fields of multiple single focus, where the electric field amplitude of a single focus is proportional to the electric field amplitude of the focus, then the total phase distribution of the multi-focus metasurface is [16]

$$\Delta\phi(x_i, y_i) = \arg\left\{ \sum_{n=1}^{N}\left[A_n\exp\left(-j\frac{2\pi}{\lambda}|F_n - r_i|\right)\right]\right\} \tag{2}$$

where N denotes the number of foci, A_n the relative electric field amplitude of the n-th focus, F_n the coordinate of focus, and r_i the metasurface unit coordinate. According to Equation (2), the number of foci N and the three-dimensional coordinates (F_{nx}, F_{ny}, F_{nz}) of each focus can be adjusted to achieve the control of the number of foci, where the position coordinates of each focus can be arbitrarily specified. The relative energy of each focus can be distributed by setting the ratio of $A_1, A_2, \ldots, A_n$.

$$\Delta\phi^{acq}(x_i, y_i) = \begin{cases} 90°, & \mathrm{mod}(\Delta\phi(x_i, y_i), 360°) \in [0°, 180°) \\ -90°, & \mathrm{mod}(\Delta\phi(x_i, y_i), 360°) \in [180°, 360°) \end{cases} \tag{3}$$

The phase distribution of the metasurface obtained from Equation (2) is continuous. For the 1-bit metasurface, the phase difference between the elements is $0°$ or $180°$. Equation (3) is used to digitally discrete the obtained phase distribution, where $-90°$ is set as "0" unit, and $90°$ degree is set as "1" unit. In order to meet most application scenarios in reality, we studied three types of focusing, as shown in Figure 1, including linear focusing, multi-focus focusing, and energy distribution design.
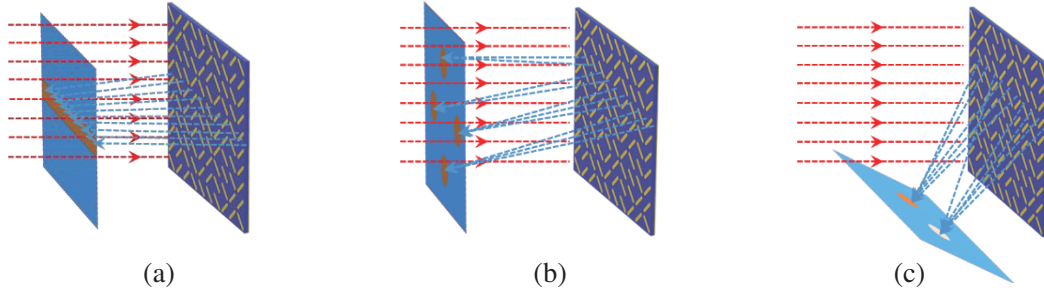

(a)   (b)   (c)

Figure 1. Schematic diagram of multi-types focusing metasurfaces. (a) Linear focusing metasurface. (b) Multi-focus metasurface. (c) Multi-focus with different intensity.

3. METASURFACE DESIGN

To verify the theoretical analysis above on multi-focus design, a 1-bit units structure is designed. The metasurfaces are arranged according to Equations (2) and (3), which combine linear focus, the number of foci, and energy distribution.

3.1. DESIGN OF 1BIT METASURFACE UNIT

In order to satisfy the 1-bit coding mode, the phase difference between the two units should be kept at $180°$. In addition, the unit should have the characteristics of broadband and high efficiency. The central frequency f_0 is 15 GHz, and the corresponding wavelength λ_0 is 20 mm. The dipole structure is adopted as unit cell, as shown in Figure 2. Each unit is composed of three layers as the "metal-medium-metal" structure. The medium material is F4B ($\varepsilon_r = 2.65$, $\tan\delta = 0.001$) with thickness (h) of $0.15\lambda_0$. The thickness of the metal layer is 0.035 mm. The top layer is a metal patch structure with length $l = 0.35\lambda_0$ and width $w = 0.07\lambda_0$, and both ends of the patch are semicircle metal with radius $w/2 = 0.035\lambda_0$. R_{xx} is defined as the reflection coefficient under x-polarization incident and x-polarization reflection (co-polarization reflection coefficient), while R_{yx} is the reflection coefficient under x-polarization incident and y-polarization reflection (cross-polarization reflection coefficient).
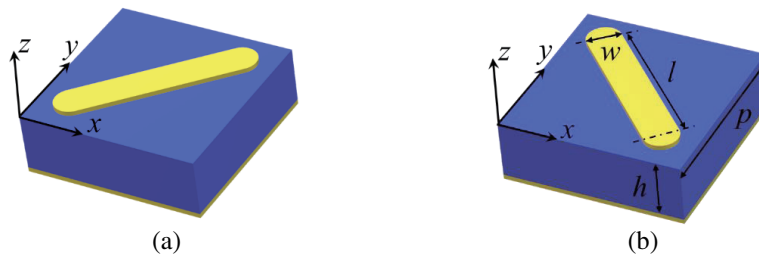

(a)   (b)

Figure 2. Focusing metasurface unit. (a) "0" element. (b) "1" element.

The Floquet port is applied to simulate the unit in commercial simulation software CST. We use the unit cell boundary to simulate an infinite period unit. The x-polarized EM wave is incident along the direction of $-z$, and the reflection phase and amplitude characteristics of the metasurface element are shown in Figure 3. It can be observed that the cross-polarization reflection amplitude is greater than
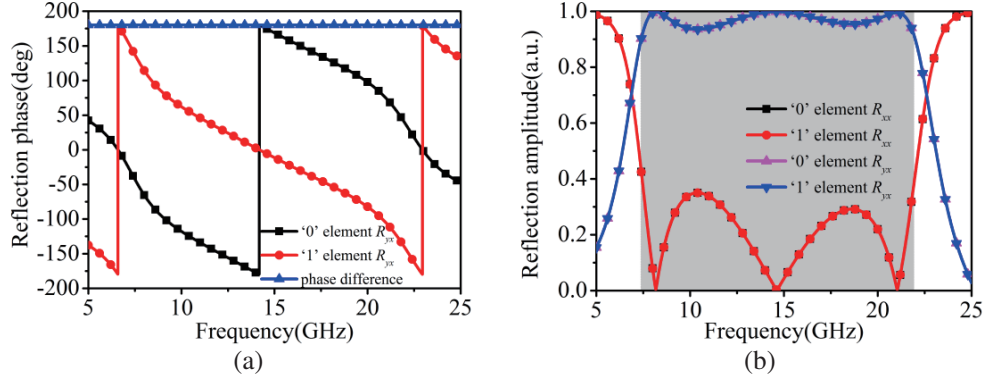
Figure 3. Reflection responses of 1-bit unit. (a) The amplitude responses of the units. (b) The phase responses of the units.

90% from 7.4 GHz to 21.9 GHz, and resonance frequency is 7.6 GHz, 14.8 GHz, and 20.8 GHz. In the working frequency band, the reflection phase difference of the element is maintained at 180°, as shown in Figure 3(b). The unit structure has good reflection amplitude and reflection phase characteristics, which is very important in the performance of coding metasurface.

3.2. METASURFACE DESIGN AND PERFORMANCE ANALYSIS

With the structure shown in Figure 2, different types of coding sequences have been designed to study the linear focusing, the number of foci, and the energy distribution. As we all know, the larger the size of the metasurface is, the better the focusing effect is. Considering the focusing effect and simulation efficiency comprehensively, the dimension of the designed metasurface is set as $240 \times 240 \, \text{mm}^2$ ($11.84\lambda \times 11.84\lambda$ at 14.8 GHz). The array is composed of 30×30 units. According to the focusing type, the corresponding formula is selected to calculate the coding sequence of the focusing metasurface. The designed metasurfaces are constructed and simulated in CST Microwave Studio. The boundary condition of array simulation is open (add space). When the x-polarized wave is incident vertically at the operating frequency 14.8 GHz, the focusing effect can be obtained by observing the amplitude distribution of the y-polarized electric field of the reflected wave. The reference origin is the center of the metasurface.

Linear focusing is actually a 1-dimensional focusing. If the focal spot is parallel to the y-axis, Equation (1) can be transformed as

$$\Delta\phi(x_i, y_i) = \arg\left\{A\exp\left(-j\frac{2\pi}{\lambda}\sqrt{(F_x - x_i)^2 + F_z^2}\right)\right\} \tag{4}$$

where F_x and F_z are the x-coordinate and z-coordinate of focal spot. If the focal spot is parallel to the x-axis, then Equation (1) deforms as

$$\Delta\phi(x_i, y_i) = \arg\left\{A\exp\left(-j\frac{2\pi}{\lambda}\sqrt{(F_y - x_i)^2 + F_z^2}\right)\right\} \tag{5}$$

If the focal spot parallel to the x-axis and y-axis exists at the same time, Equation (2) can be expressed as

$$\Delta\phi(x_i, y_i) = \arg\left\{A_1\exp\left(-j\frac{2\pi}{\lambda}\sqrt{(F_{1x} - x_i)^2 + F_{1z}^2}\right) + A_2\exp\left(-j\frac{2\pi}{\lambda}\sqrt{(F_{2y} - x_i)^2 + F_{2z}^2}\right)\right\} \tag{6}$$

Equations (4)–(6) give the continuous phase distribution on the metasurface, so it is necessary to use Equation (3) for phase quantization. Then, $-90°$ is set as "0" unit, and $90°$ degree is set as "1" unit. Use the designed 1bit unit to arrange the whole metasurface.

The schematic diagram of the metasurface and the corresponding coordinate axes are shown in Figure 4(j). The origin of the coordinate axis is at the center of the metasurface. All the focal length
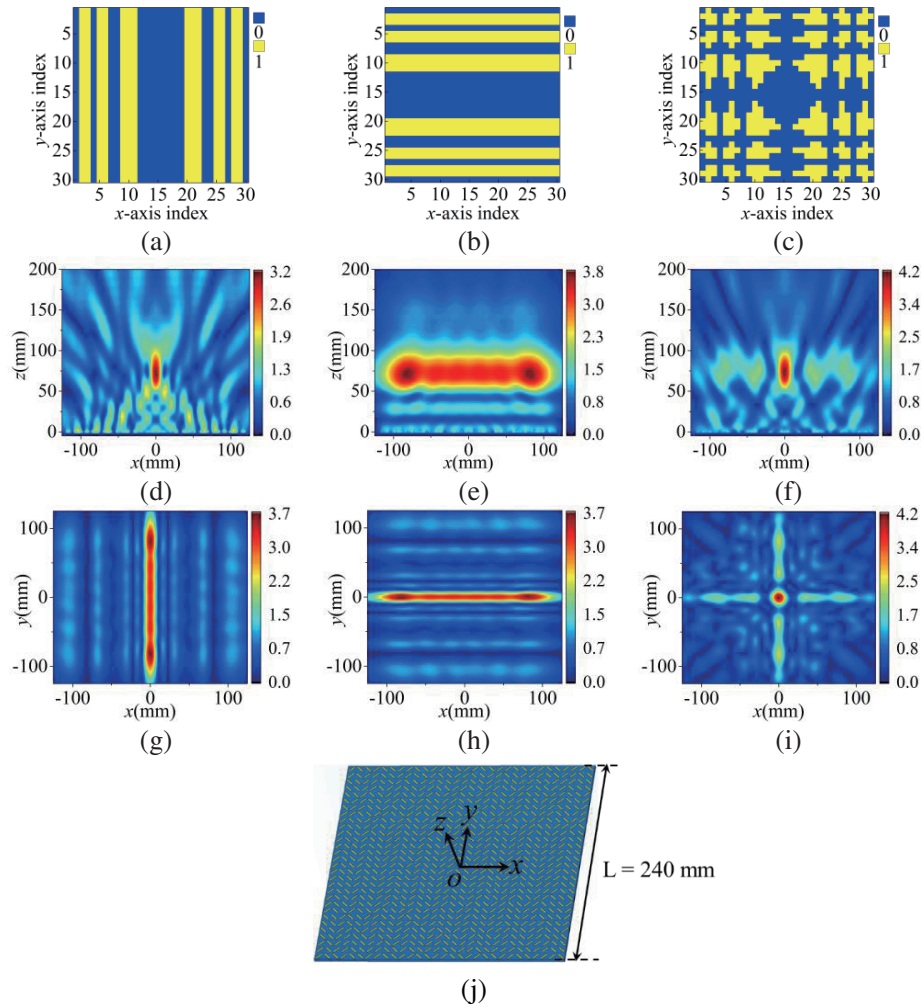
Figure 4. Coding sequences for linear focus and simulated near-field amplitude distribution in different planes. (a) Coding sequence calculated by (4) when $F_x = 0$ mm and $F_z = 75$ mm. (b) Coding sequence calculated by (5) when $F_y = 0$ mm and $F_z = 75$ mm. (c) Coding sequence calculated by (6) when $F_{1x} = 0$ mm, $F_{1y} = 0$ mm, and $F_z = 75$ mm. (d)–(f) Amplitude distributions in xoz plane at $y = 0$ mm for (a)–(c). (g)–(i) Amplitude distributions in xoy plane at $z = 75$ mm for (a)–(c). (j) Schematic diagram of metasurface and corresponding coordinate axis.

is set as 75 mm, and the coding sequence corresponding to the three types of linear focal spots was calculated according to Equations (4), (5), and (6), as shown in Figures 4(a), 4(b), and 4(c). The electric field intensity of the incident wave is set as 1 V/m, and the electric field amplitude of y-polarization is observed in the xoz and xoy planes. When there is only one focal spot, the focal length is close to the set value, and the maximum electric field intensity at the focal spot is 3.8 V/m, which is 3.8 times of the incident intensity, as shown in Figures 4(d)–4(i). This shows that the focusing metasurface has a good linear focusing effect. When there are two orthogonal focal spots at the same time, the electric field intensity at the intersection point becomes 4.2 V/m due to the superposition of energy.

The design method is also applied to control the performance of focusing metasurface on the number of foci. In order to observe the focusing effect, the z-coordinate of all foci is set as 180 mm. The coordinates of the two focal points are set as $(\pm42, 0, 180)$, the three focal points set as $(\pm42, -42, 180)$ and $(0, 42, 180)$, and the coordinates of the four focal points set as $(\pm42, \pm42, 180)$. Then the coding sequence is calculated by Equation (2), respectively, as shown in Figures 5(a)–5(c). According to the coding sequence, the simulation model is built in CST. The electric field amplitude distributions of xoy
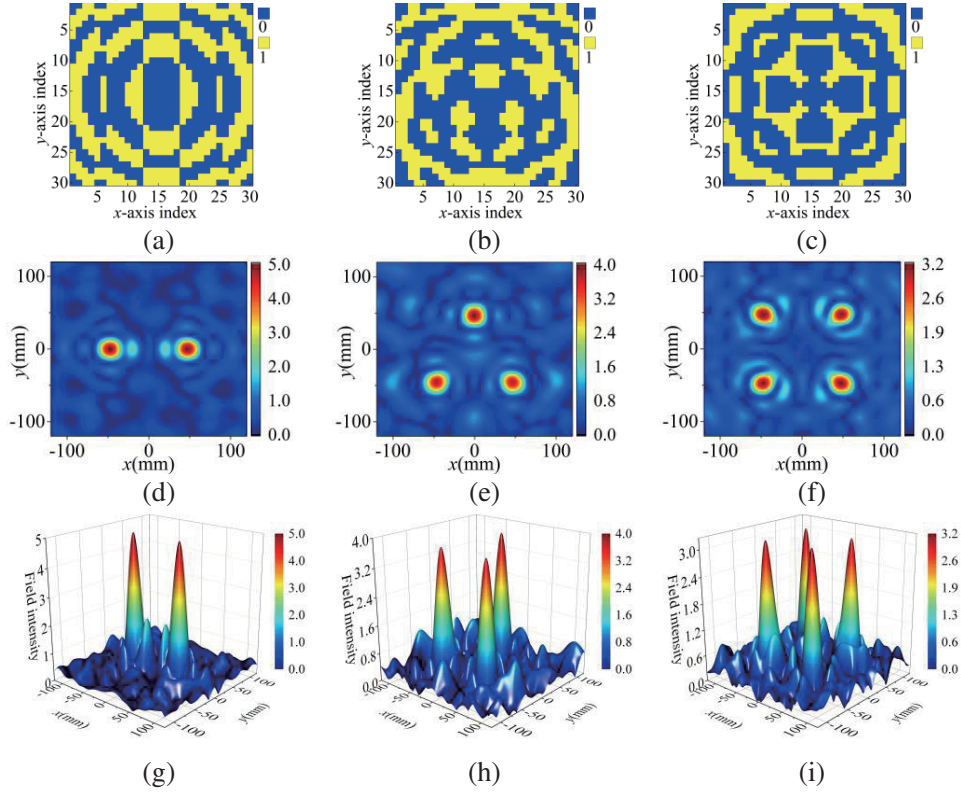
Figure 5. Coding sequences for different number of focus and simulated electric field amplitude distribution in *xoy* planes.
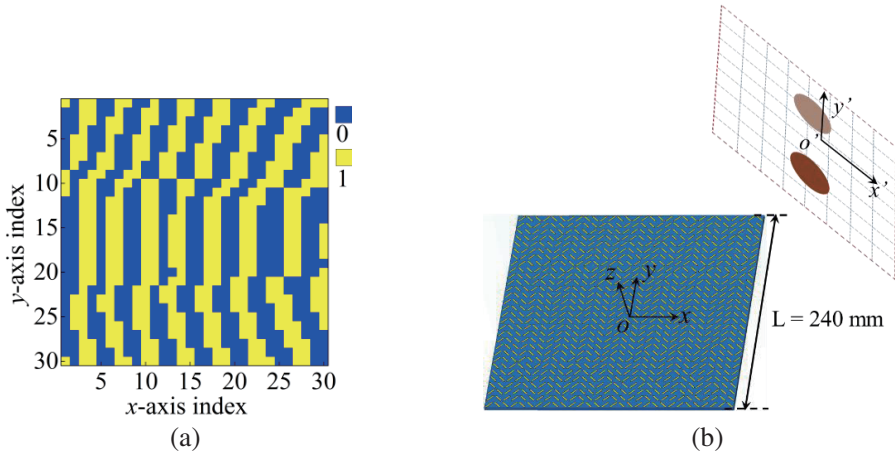

Figure 6. Schematic diagram of metasurface generating two focus with unequal power division. (a) Coding sequence for generating two focus with different intensity. (b) Sampling diagram.

plane with $z = 180$ mm under three conditions were observed respectively. As shown in Figures 5(d)–5(i), with the increase in the number of focal points, the maximum electric field amplitude at the focal point is 3.2 V/m, 4 V/m, and 5 V/m, respectively. All focal coordinates are equal to the set value, indicating that this method can effectively regulate the number of foci.

To further verify the performance of the design method on the focus position and energy distribution, the superposition principle of the field is used to design two-focus metasurface with unequal energy. The three-dimensional coordinate of the two foci was set as $(260, \pm 50, 260)$, and the electric

field amplitude ratio at the focal point $A_1 : A_2 = 4 : 5$. The coding sequences are calculated from Equations (3) and (4), as shown in Figure 6(a). The amplitude of the y-polarized electric field in the plane is shown in Figure 6(b). The origin of plane $x'o'y'$ is (260, 0, 260) of the original xoy coordinate, and the angle between the observed plane and the metasurface is set as 45°.

Figures 7(a) and 7(b) are the amplitude distribution of y-polarization electric field in the xoz plane with $y = \pm 50$ mm. It can be seen that the z-coordinates of both focal points are 262 mm, which is very close to the preset value of 260 mm. Figures 7(c) and (d) are the electric field amplitude distribution in the $x'o'y'$ plane. The y-coordinate of the focus is ± 49 mm, which is very close to the preset value of ± 50 mm. The simulated results show that this approach can precisely regulate the position of the focus. The maximum amplitude ratio of bifocal point is $1.7 : 2.67 = 1 : 1.57$, which is also close to the preset value $4 : 5 = 1 : 1.25$, indicating that this method can regulate the energy ratio of the two-focusing point to a certain extent.
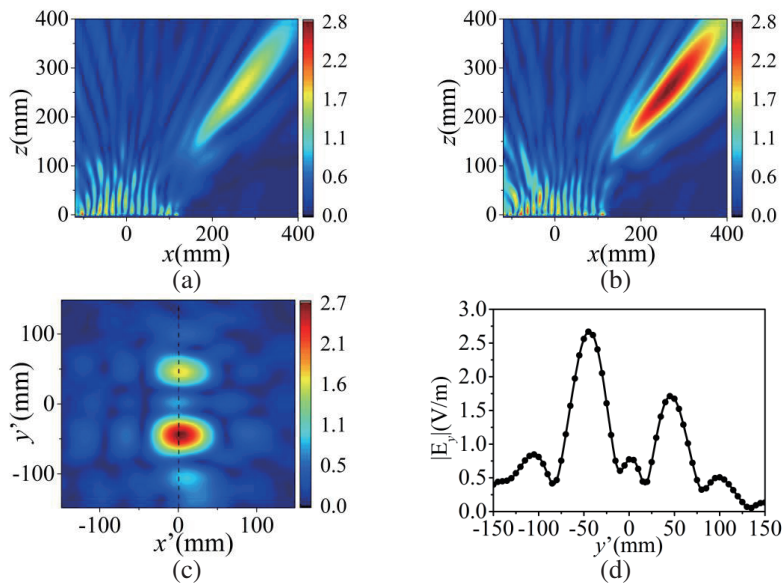

Figure 7. Amplitude distribution in different sampling planes. (a) $y = 50$ mm. (b) $y = -50$ mm. (c) The $x'o'y'$ plane in Figure 6(b). (d) The intensity on the dotted line in Figure 7(c).
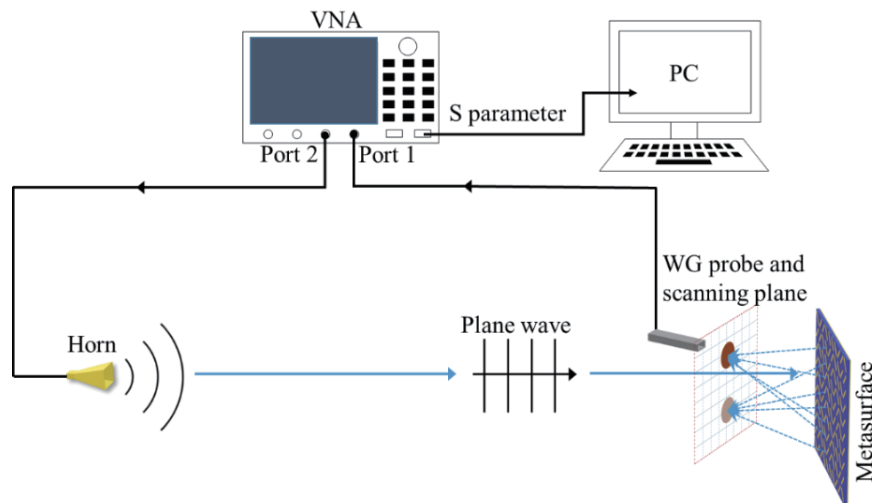

Figure 8. Experimental system diagram.

4. MEASUREMENT RESULTS

To experimentally validate the above design approach, the unequal power split two-focus metasurface is manufactured. The experimental system diagram is displayed in Figure 8. The horn is connected to port 2 of the vector network analyzer (VNA), and plane wave is adopted as the metasurface feed source. According to the antenna theory, the spherical wave emitted by the feed horn needs to pass through the propagation distance of $2L^2/\lambda$ to be equivalent to a plane wave, where L is the metasurface side length. Thus the distance between the horn and the metasurface should be greater than 5.376 m. The plane wave is reflected by the metasurface to obtain the bifocal point. Port 1 of the VNA is connected with the scanning probe. Due to the characteristics of cross polarization, vertical polarized waves are emitted from the horn, and horizontal polarized waves are received by the waveguide probe. The sampling plane of the receiving probe is clamped at a 45° to the metasurface, and the scanning range is $140 \times 140\,\mathrm{mm}^2$ in $x'o'y'$ plane with a step of 2 mm. The measurement environment and metasurface prototype are shown in Figures 9(a) and (b), respectively.
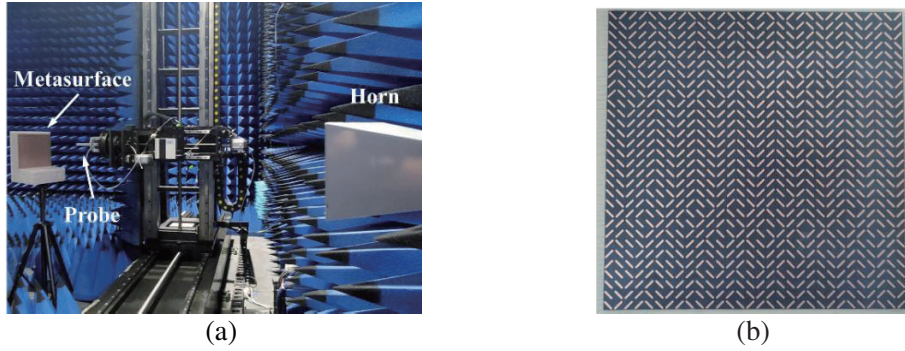

Figure 9. (a) Measurement environment. (b) Metasurface prototype.

The measurement results are shown in Figure 10. It can be seen that the coordinates of $x'o'y'$ of the bifocal point are $(12, \pm62)$, which are different from the simulation results of $(0, \pm49)$. The reason for this situation is that the relative positions of the metasurface and the scanning rack are artificially placed, and the receiving probes move horizontally and vertically, so systematic errors will inevitably exist in the measuring process. The bifocal energy ratio is $1.5 : 2.3 = 1 : 1.53$, as shown in Figure 10(b), which coincides with simulation. In general, the number of near-field multi-focal points can be strictly controlled by the 1-bit coded metasurface designed using the principle of electric field superposition. It can also control the focus position of each focus more accurately. However, due to the large phase
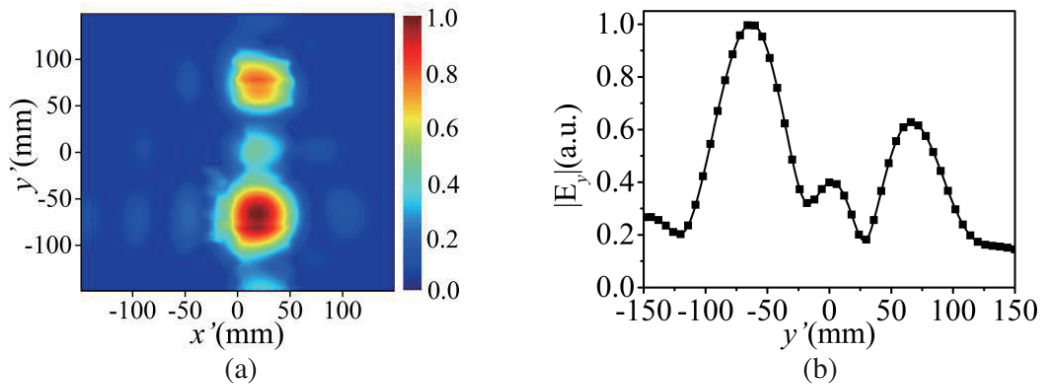

Figure 10. Measurement results of two-focus metasurface. (a) Distribution of electric field amplitude in $x'o'y'$ plane. (b) Measured intensity ratio of the two focus.

quantization error caused by 1-bit encoding, the accuracy of energy allocation for each focus needs to be improved. In the later research, it can be considered to increase the coding bit to improve the energy allocation accuracy.

5. CONCLUSION

In summary, we have proposed and verified the method of the superposition principle of electric field vector to form MTF, which can realize linear focusing, multi-focus focusing, and unequal power division focusing. According to the focusing type, the coding sequence of the 1-bit metasurface could be calculated easily and flexibly. By using a dipole antenna structure, 1-bit unit is designed, and then two, three, and four-focus focusing metasurfaces and two-focus energy distribution metasurfaces are simulated in CST, respectively. The bifocal power distribution metasurface is fabricated and measured, and the measurement results, theoretical derivation, and simulation results are consistent with each other. The feasibility and effectiveness of the focusing metasurface design method are verified theoretically and experimentally. It has the advantages of simple design, thin thickness, and ease of fabrication, and can be applied in fields such as RFID, microwave imaging, and wireless power transmission.

REFERENCES

1. Li, P., M. Lewin, A. V. Kretinin, et al., "Hyperbolic phonon-polaritons in boron nitride for near-field optical imaging," *Nature Communications*, Vol. 6, 7507, 2015.
2. Buffi, A., A. A. Serra, P. Nepa, et al., "A focused planar microstrip array for 2.4 GHz RFID readers," *IEEE Transactions on Antennas and Propagation*, Vol. 58, No. 5, 1536–1544, 2010.
3. Zhao, J., H. Ye, K. Huang, et al., "Manipulation of acoustic focusing with an active and configurable planar metasurface transducer," *Scientific Reports*, Vol. 4, 6257, 2013.
4. Grbic, A. and R. Merlin, "Near-field focusing plates and their design," *IEEE Transactions on Antennas and Propagation*, Vol. 56, No. 10, 3159–3165, 2008.
5. Fennell, R. D., M. Sher, and W. Asghar, "Design, development, and performance comparison of wide field lensless and lens-based optical systems for point-of-care biological applications," *Optics and Lasers in Engineering*, Vol. 137, 106326, 2021.
6. Bogosanovic, M. and A. G. Williamson, "Microstrip antenna array with a beam focused in the near-field zone for application in noncontact microwave industrial inspection," *IEEE Transactions on Instrumentation and Measurement*, Vol. 56, No. 6, 2186–2195, 2007.
7. Bao, L., R. Y. Wu, X. Fu, et al., "Multi-beam forming and controls by metasurface with phase and amplitude modulations," *IEEE Transactions on Antennas and Propagation*, Vol. 67, No. 10, 6680–6685, 2019.
8. Zhang, L., Z. X. Wang, R. W. Shao, et al., "Dynamically realizing arbitrary multi-bit programmable phases using a 2-bit time-domain coding metasurface," *IEEE Transactions on Antennas and Propagation*, Vol. 68, No. 4, 2984–2992, 2019.
9. Parinaz, N., S. A. Matos, et al., "Dual-band dual-linear-to-circular polarization converter in transmission mode application to K/Ka -Band satellite communications," *IEEE Transactions on Antennas and Propagation*, Vol. 66, No. 12, 7128–7137, 2018.
10. Yu, N., P. Genevet, M. A. Kats, et al., "Light propagation with phase discontinuities reflection and refraction," *Science*, Vol. 334, No. 6054, 333–337, 2011.
11. Abdulkarim, Y. I., H. N. Awl, F. F. Muhammadsharif, et al., "A low-profile antenna based on single-layer metasurface for Ku-band applications," *International Journal of Antennas and Propagation*, 8813951, 2020.
12. Afzal, M. U. and K. P. Esselle, "Recent advances in near-field meta-steering," *2020 IEEE International Symposium on Antennas and Propagation and North American Radio Science Meeting*, IEEE, 2020.

13. Zhang, P., L. Li, X. Zhang, et al., "Design, measurement and analysis of near-field focusing reflective metasurface for dual-polarization and multi-focus wireless power transfer," *IEEE Access*, Vol. 7, 10387–110399, 2019.

14. Lv, Y. H., X. Ding, B. Z. Wang, et al., "Wideband polarization-insensitive metasurface with tunable near-field scattering focusing characteristic," *Electronics Letters*, Vol. 55, No. 14, 776–778, 2019.

15. Fan, J. and Y. Cheng, "Broadband high-efficiency cross-polarization conversion and multi-functional wavefront manipulation based on chiral structure metasurface for terahertz wave," *Journal of Physics D: Applied Physics*, Vol. 53, No. 2, 025109, 2020.

16. Yu, S., H. Liu, et al., "Design of near-field focused metasurface for high-efficient wireless power transfer with multifocus characteristics," *IEEE Transactions on Industrial Electronics*, Vol. 66, No. 5, 3993–4002, 2019.

17. Wan, X., Q. Zhang, T. Y. Chen, et al., "Multichannel direct transmissions of near-field information," *Light: Science & Applications*, Vol. 8, No. 1, 60, 2019.

18. Cui, T. J., Q. Q. Mei, X. Wan, et al., "Coding metamaterials, digital metamaterials and programming metamaterials," *Light: Science & Applications*, Vol. 3, No. 10, e218, 2014.

19. Ozdemir, E., O. Akgol, F. O. Alkurt, et al., "Mutual coupling reduction of cross-dipole antenna for base stations by using a neural network approach," *Applied Sciences*, Vol. 10, No. 1, 378, 2020.

20. Alkurt, F. O., M. E. Ozdemir, O. Akgol, et al., "Ground plane design configuration estimation of 4.9 GHz reconfigurable monopole antenna for desired radiation features using artificial neural network," *International Journal of RF and Microwave Computer-Aided Engineering*, Vol. 32, No. 8, e22734, 2021.

21. Afzal, M. U., et al., "A low-profile printed planar phase correcting surface to improve directive radiation characteristics of electromagnetic band gap resonator antennas," *IEEE Transactions on Antennas & Propagation*, Vol. 64, No. 1, 276–280, 2016.

22. Guo, W.-L., G.-M. Wang et al., "Multi-functional coding metasurface for dual-band independent electromagnetic wave control," *Optics Express*, Vol. 27, No. 14, 19196–19211, 2019.